Clinical Neurophysiology 190 (2026) 2112327

Contents lists available at ScienceDirect

Clinical Neurophysiology

journal homepage: www.elsevier.com/locate/clinph

# Test-retest reliability of early TMS-evoked potentials over fMRI-based definitions of non-motor targets

Ceyda Sayalı [a,*], Juha Gogulski [b,c], Ida Granö [b], Daniel Jaro [a], Eli Weisman [a], Gabriela Lofland [a], Pantelis Lioumis [b,d,1], Frederick S. Barrett [a,1]

[a] Center for Psychedelic and Consciousness Research, Dept of Psychiatry and Behavioral Sciences, Johns Hopkins University School of Medicine, Baltimore, MD, USA
[b] Department of Neuroscience and Biomedical Engineering, Aalto University School of Science, Espoo, Finland
[c] Department of Clinical Neurophysiology, HUS Diagnostic Center, Clinical Neurosciences, Helsinki University Hospital and University of Helsinki, Helsinki, Finland
[d] BioMag Laboratory, HUS Medical Imaging Center, Helsinki University Hospital, Helsinki, Finland

A B S T R A C T

*Objective:* This study assessed the test–retest reliability of TMS-evoked potentials (TEPs) across two cortical regions—dorsolateral prefrontal cortex (DLPFC), and angular gyrus—in comparison to motor cortex (M1), using individualized and literature-based targeting approaches. The study also compared the reliability of different double-pulse TMS protocols.

*Methods:* Seventeen healthy participants underwent two TMS-EEG sessions spaced by at least one week, with targets for DLPFC and angular gyrus identified using resting-state functional connectivity (RS) and Neurosynth-based functional overlays.

*Results:* M1 demonstrated the highest TEP reliability (Concordance Correlation Coefficient (CCC) mean = 0.59), while DLPFC (CCCmean = 0.40) and angular gyrus (CCCmean = 0.45) showed lower reliability, particularly for anterior DLPFC targets. Neurosynth-based DLPFC targets exhibited slightly higher CCC values (mean CCC = 0.57) compared to RS-based targets (mean CCC = 0.30), but the difference was not statistically significant. No significant differences in reliability were found across TMS protocols.

*Conclusion:* While fMRI-based targeting optimizes the engagement of functional networks, TMS-EEG needs to prioritize signal-to-noise ratio (SNR) to minimize artifacts and maximize reliability.

*Significance:* This work bridges the gap between fMRI-guided targeting and TMS-EEG applications.

## 1. Introduction

Transcranial magnetic stimulation (TMS) enables precise manipulation of brain activity, with measurable effects on behavior and cognition (Sack et al., 2006; Hallett, 2000; Pascual-Leone et al., 2000). With the expanding use of TMS, several methods for determining target stimulation sites have emerged. These include targeting based on anatomical brain structures, which involves positioning the TMS coil over regions identified through anatomical landmarks (Wilson et al., 1993; Krings et al., 1997; Boroojerdi et al., 1999). Other approaches use coordinates in standardized brain atlas space, which rely on group-level averages derived from the literature, or electroencephalograph (EEG) electrode positioning (Herwig et al., 2003; Fitzgerald et al., 2009; Beam et al., 2009; Rusjan et al., 2010). Finally, individualized coordinates, typically derived from identifying peak resting- or task-based activations in functional magnetic resonance imaging (fMRI) or by identifying anatomical landmarks using structural MRI, allow for more precise targeting by accounting for each participant's unique functional or structural brain anatomy (Paus et al., 1997; Balderston et al., 2022; Oathes et al., 2021; Beynel et al., 2024). Although each method varies in accuracy, individualized approaches might be expected to generally provide more reliable and effective outcomes in terms of engaging the intended brain regions and producing measurable effects (Fitzgerald et al., 2009; Sack et al., 2009; Sparing et al., 2008).

Evidence to date suggests the potential value in using fMRI measures in particular to guide TMS targeting. For example, individualized targeting based on each person's resting-state functional connectivity may be particularly beneficial for precise TMS application in the dorsolateral prefrontal cortex (DLPFC; Fox et al., 2012). The DLPFC is a primary target in treatment of major depressive disorder (MDD), where therapeutic outcomes have been linked to functional connectivity between the DLPFC stimulation site and the subgenual cingulate cortex (Cash et al., 2021). A standard protocol for the MDD treatment involves targeting repetitive TMS to the DLPFC based on a location 5.5 cm anterior

* Corresponding author at: 5510 Nathan Shock Dr, Baltimore, MD 21224, USA.
*E-mail address:* zsayali1@jhmi.edu (C. Sayalı).
[1] Indicates shared senior authorship.

https://doi.org/10.1016/j.clinph.2026.2112327
Accepted 27 June 2026
Available online 3 July 2026
1388-2457/© 2026 International Federation of Clinical Neurophysiology. Published by Elsevier B.V. All rights are reserved, including those for text and data mining, AI training, and similar technologies.

to the site used to identify a given patient's motor threshold (Horvath et al., 2010). However, this does not take into account rich, well-described, and expected individual variability in structural and functional anatomy of the prefrontal cortex (Steinmetz and Seitz, 1991; Hoshi, 2006; Cieslik et al., 2013, 2016). Fox et al. (2012) observed large, reproducible individual differences in DLPFC resting-state functional connectivity across sessions, supporting the potential for such connectivity measures for targeting of personalized stimulation.

A seminal study by Sack et al. (2009) demonstrated that individualized fMRI-guided TMS significantly increases the likelihood of both neural and behavioral engagement in cognitive studies. This approach led to stronger effects with fewer participants, as only five subjects were required to observe a behavioral effect when using individualized fMRI-based targeting. In contrast, twice as many participants were needed with structural MRI or group-analyzed fMRI, and 47 participants were necessary when using standardized spatial coordinates, such as the electrode locations in the 10/20 EEG system. These findings underscore the likelihood of increased variability when targeting TMS with standardized methods and reinforce the necessity of individualized approaches for robust outcomes. Since then, cognitive neuroscience has increasingly relied on fMRI-based targeting to engage specific brain regions, including subcortical structures, in studies of both brain function and behavior (Oliver et al., 2022; Oathes et al., 2021; Hawco et al., 2018; Dengler et al., 2024; Nord, 2021; Nee and D'Esposito, 2017; Desrochers et al., 2015).

In parallel, EEG measurement during TMS stimulation (TMS-EEG) has emerged as an advanced technique for non-invasive probing of brain function, providing insights into excitation, inhibition, oscillatory activity, connectivity, and plasticity in both healthy and clinical populations (Ilmoniemi et al., 1997; Tremblay et al., 2019; Hernandez-Pavon et al., 2023). TMS-EEG has been proven reproducible (Lioumis et al., 2009; Casarotto et al., 2010; Kerwin et al, 2018), making this a powerful method for exploring neurophysiological function in cortical regions without direct motor and behavioral outputs such as the DLPFC, which is implicated in several clinical disorders (Rogasch et al., 2015; Farzan et al., 2009; Ferrarelli and Phillips, 2021; Lioumis et al., 2009; Daskalakis et al., 2008; Canali et al., 2015; Radhu et al., 2016, 2017; Noda et al., 2017). TMS-EEG methods have advanced our understanding of GABAergic dysfunction in MDD and schizophrenia (Hui et al., 2020), identifying abnormalities that may serve as both biomarkers and therapeutic targets (Rogasch et al., 2015). Furthermore, TMS-EEG has been shown to predict treatment responses in mood disorders and identify biomarkers in disorders of consciousness and epilepsy, highlighting its clinical utility (Sun et al., 2016; Canali, 2014; Canali et al., 2017; Casarotto et al., 2013; Pellicciari et al., 2017; Casali et al., 2013; Casarotto et al., 2017; Bodart et al., 2017; Valentin et al., 2008; Shafi et al., 2016).

However, TMS-EEG studies have taken a different route from TMS-fMRI research. Unlike the individualized fMRI approaches commonly used in TMS-fMRI studies, TMS-EEG research has largely relied on standardized targeting methods such as EEG electrode placement (Fox et al., 2012; Herwig et al., 2003; Herbsman et al., 2009; Harquel et al., 2016; Weigand et al., 2018). Importantly, target selection in TMS-EEG studies (Casarotto et al., 2022; Lioumis and Rosanova, 2022) poses specific challenges in data reliability, as EEG is particularly prone to TMS-induced artifacts such as large transient electrical signals, limits to amplifier recovery time that are strained by TMS-induced artifacts, electrical recharging artifacts, and muscle artifacts, specifically affecting regions surrounding cranial muscles (Mäki and Ilmoniemi, 2011; Mutanen et al., 2013; Veniero et al., 2009). Other issues include TMS-induced electrode movement, heating of electrodes from repeated stimuli, and sensory responses that may be misinterpreted as TMS-evoked brain activity. Even minor shifts in coil positioning can result in substantial changes in the evoked signals, making precise targeting crucial for reliable outcomes (Komssi et al., 2002; Casarotto et al., 2010).

While TMS-EEG has been applied in repeated measures designs to assess the impact of interventions, the test–retest reliability of TMS-evoked EEG potentials has not been well-described, particularly across different TMS targeting methods, raising concerns about whether reliability varies depending on the targeting approach or remains unknown altogether. Few studies have investigated the reproducibility and reliability of single-pulse TMS-EEG (Gogulski et al., 2024a; Lioumis et al., 2009; Casarotto et al., 2010; Kerwin et al., 2018; Conde et al., 2019), and those that have typically used EEG cap placement to guide TMS targeting. Additionally, studies show that targeting different subregions within the same brain area, such as the DLPFC, can significantly impact the reliability of TMS-evoked potentials (Gogulski et al., 2024a). For instance, posterior and medial DLPFC targets produce larger and more reliable TEPs compared to anterior targets, where artifacts from muscle activation often mask the true neural response (Gogulski et al., 2024a).

Given the evidence for functional and structural anatomical variability in the cortex and implications of this variability for both non-invasive brain stimulation and cognition, this study examines whether literature-based or individually defined fMRI-based targets yield reliable TEPs. To assess the test–retest reliability of TEPs in different cortical regions, we employed distinct targeting approaches based on the unique characteristics of each region. The motor cortex was targeted using the resting motor threshold (RMT) procedure due to its well-defined functional readout via muscle movement, providing a benchmark for reliability. In contrast, DLPFC and angular gyrus lack such direct functional outputs, necessitating the use of alternative targeting methods to evaluate TEP reliability. By comparing these methods in non-motor regions, we aim to understand the reliability of TEPs in networks associated with these regions and gain insight into their underlying function. This multi-region approach contextualizes the motor cortex as a reference point and frames the exploration of test–retest reliability in regions without readily observable functional markers.

Specifically, we assess the test–retest reliability of early (20–60 ms) TEPs across three brain regions: the motor cortex (serving as a control region known for high reliability, identified through EMG and motor thresholding based on anatomical landmarks), the left DLPFC, and the left angular gyrus. The DLPFC and angular gyrus were selected as cortical sites accessible by TMS within the frontoparietal network (FPN) and the default mode network (DMN), respectively, as defined by resting-state connectivity analyses (Yeo et al., 2011). The DLPFC was selected due to its frequent use as a target for TMS in depression treatment, where stimulation in this region has consistently shown efficacy in modulating mood-related networks. The angular gyrus was chosen for its role within the DMN, which is implicated in self-referential thinking and social cognition. Disruptions in DMN connectivity are associated with depressive symptoms, such as rumination, which impact treatment outcomes (Buckner et al., 2008). Left-lateral regions were chosen given that approved rTMS therapies target left-lateral regions. We compared the reliability of TMS responses across all sites using three TMS protocols (single pulse, SICI, ICF). We also compared the reliability of TMS response across two target definitions—one based on resting-state (RS) fMRI and the other on Neurosynth overlays on anatomical images—for the DLPFC and angular gyrus.

## 2. Materials and methods

### 2.1. Participants

Eighteen healthy participants participated in the study. One participant did not complete the second TMS-EEG session, and their data was excluded from the analysis. Seventeen participants ($M_{age} = 28$, $SD_{age} = 6.28$, 8 women and 9 men) completed all study procedures. Participants with psychiatric or neurological disorders (including moderate or severe depression), recent substance use disorder, cardiac events, pregnancy, contraindications for TMS or MRI, or a lifetime history of psychotropic medication use were excluded. The study's experimental procedures

were approved by the Johns Hopkins University Institutional Review Board. All participants provided written informed consent before the experiment.

### 2.2. Design

After a baseline MRI acquisition, the study followed a repeated-measures design, with participants visiting the lab on two separate occasions separated by at least one week (Fig. 1A). All TMS-EEG procedures were repeated at each visit. To ensure consistency, each session began at the same time of day for both visits.

### 2.3. MRI acquisition

Individual anatomical images required for 3D reconstruction and neuronavigation were obtained for each participant using a Philips Achieva 3 T MRI scanner and a 32-channel head coil. A T1-weighted MPRAGE image was acquired for each participant, with a slice thickness of 1 mm, no slice gap, and a 256 × 256 matrix in sagittal orientation. Resting-state BOLD images were also collected to analyze intrinsic brain connectivity, with the following parameters: multi-slice (MS) gradient-echo planar imaging (EPI), Repetition Time (TR) of 800 ms, 910 volumes for a total scan time of 12:08, Echo Time (TE) of 30 ms, flip angle of 52°, slice thickness of 2.4 mm without slice gap, and in-plane resolution of 2.25 $mm^2$. Posterior to anterior and an anterior to posterior field maps were also acquired at the same resolution as the BOLD images to correct for distortion artifacts.

### 2.4. MRI preprocessing

MRI data were organized using BIDS format (Gorgolewski et al., 2017) and preprocessed using fMRIPrep 21.0.4 (Esteban et al. (2018); Esteban, Blair, et al. (2018); RRID:SCR_016216), which is based on Nipype 1.6.1 (Gorgolewski et al. (2011); Gorgolewski et al. (2017); RRID:SCR_002502).

### 2.5. Anatomical data preprocessing

The anatomical image for each participant was corrected for intensity non-uniformity (INU) using N4BiasFieldCorrection (Tustison et al., 2010), as distributed with ANTs 2.3.3 (Avants et al., 2008), and used as the anatomical reference throughout the workflow. The anatomical reference was then skull-stripped using a Nipype implementation of the antsBrainExtraction.sh workflow from ANTs, with OASIS30ANTs as the target template.

Brain tissue segmentation of cerebrospinal fluid (CSF), white matter (WM), and gray matter (GM) was performed on the skull-stripped anatomical image using fast [FSL 6.0.5.1]. Brain surfaces were reconstructed using recon-all [FreeSurfer 6.0.1; Dale et al., 1999]. The brain mask estimated previously was refined with a custom method to reconcile ANTs-derived and FreeSurfer-derived segmentations of the cortical gray matter, as implemented in Mindboggle (Klein et al., 2017).

Volume-based spatial normalization to a standard space (using the MNI152NLin2009cAsym template) was performed through nonlinear registration with antsRegistration (ANTs 2.3.3), using brain-extracted versions of both the T1w reference and the T1w template.

### 2.6. Functional data preprocessing

For the BOLD run for each participant, a reference volume and its skull-stripped version were generated using a custom methodology of fMRIPrep. Head-motion parameters with respect to the BOLD reference (transformation matrices and six corresponding rotation and translation parameters) were estimated before any spatiotemporal filtering using mcflirt [FSL 6.0.5.1:57b01774, Jenkinson et al., 2002]. The BOLD time-series (including slice-timing correction) was then resampled to their original, native space by applying transforms to correct for head motion. These resampled BOLD time-series will be referred to as preprocessed BOLD in original space, or simply preprocessed BOLD.

The BOLD reference was then co-registered with six degrees of freedom to the anatomical reference using bbregister (FreeSurfer), which implements boundary-based registration (Greve and Fischl, 2009). Resampling was performed in a single interpolation step by composing all pertinent transformations (i.e., head-motion transform matrices, susceptibility distortion correction from fieldmaps, and co-registrations to anatomical and output spaces). Volumetric (gridded) resampling was performed using antsApplyTransforms (ANTs), configured with Lanczos interpolation to minimize smoothing effects from other kernels. Non-gridded (surface) resampling was performed using mri_vol2surf (FreeSurfer).

### 2.7. RS-fMRI analysis

Individual resting-state scans were analyzed separately for each

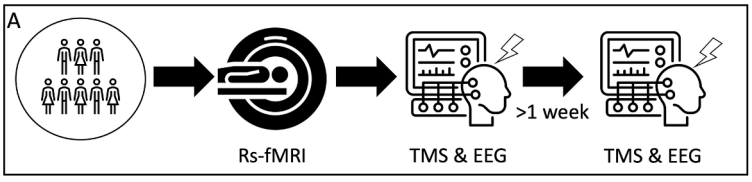


B

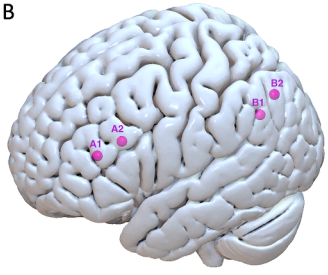


C

| Exemplar task order | | | | |
|---|---|---|---|---|
| **Protocol** | **%RMT** | **Lag (ms)** | **Region** | **Targeting method** |
| Excitation | 80-120 | 11 | DLPFC | RS |
| Single | 120 | 0 | Angular | RS |
| Single | 120 | 0 | DLPFC | NS |
| Single | 120 | 0 | Angular | NS |
| Inhibition | 80-120 | 3 | Motor | RMT |
| Inhibition | 80-120 | 3 | DLPFC | RS |
| Single | 120 | 0 | Motor | RMT |
| Single | 120 | 0 | DLPFC | RS |
| Excitation | 80-120 | 11 | Angular | RS |
| Excitation | 80-120 | 11 | Motor | RMT |
| Inhibition | 80-120 | 3 | Angular | RS |
| Single | 120 | 0 | Sham Angular | |
| Single | 120 | 0 | Sham DLPFC | |
| Single | 120 | 0 | Sham Motor | |

D

| | Regions of Interest (ROI) | |
|---|---|---|
| Small | **DLPFC** | F1, F3 |
| | **Angular Gyrus** | P1, P3 |
| | **Motor Cortex** | C1, C3 |
| Large | **DLPFC** | F1, F3, F5, FC1, FC3, FC5 |
| | **Angular Gyrus** | P1, P3, P5, CP1, CP3, CP5 |
| | **Motor Cortex** | C1, C3, C5, Cz |

E

| | Time Window |
|---|---|
| **DLPFC** | 20–60 ms |
| **Angular Gyrus** | 20–60 ms |
| **Motor Cortex** | 10–40 ms |

**Fig. 1.** Study schematic. A) Study design: Following screening, participants underwent resting-state fMRI (RS-fMRI). Subsequently, they completed two TMS-EEG sessions, scheduled at least one week apart. B) Individual connectivity- and Neurosynth-based targets for left DLPFC and left angular gyrus: A1: DLPFC_RS (−38, 39, 17), A2: DLPFC_NS (−38, 24, 24); B1: AngularGyrus_RS (−44, −58, 32), B2: AngularGyrus_NS (−46, −66, 44). C) Table depicts an exemplary sequence of experimental conditions for one subject. RMT: Resting Motor Threshold; RS: Resting State; NS: Neurosynth. D) Channels selected for small and large ROI definitions. Small ROI results are provided in the Supplemental Results (Table S1). E) Time windows chosen for each region to optimize the capture of early neural responses in each target region, facilitating a comparison of TEP reliability across anatomically defined ROIs.

participant using Independent Component Analysis (ICA) to identify functional connectivity networks. Analysis was carried out using Probabilistic Independent Component Analysis [Beckmann, 2004] as implemented in MELODIC (Multivariate Exploratory Linear Decomposition into Independent Components) Version 3.15, part of FSL (FMRIB's Software Library, www.fmrib.ox.ac.uk/fsl).

The following pre-processing steps were applied to the input data: masking of non-brain voxels, voxel-wise demeaning of the data, and normalization of the voxel-wise variance. Pre-processed data were then whitened and projected into a 15-dimensional subspace using Principal Component Analysis.

The whitened observations were decomposed into sets of vectors that describe signal variation across the temporal domain (time-courses) and spatial domain (maps) by optimizing for non-Gaussian spatial source distributions using a fixed-point iteration technique (Hyvarinen, 1999). Estimated component maps were divided by the standard deviation of the residual noise and thresholded by fitting a mixture model to the histogram of intensity values (Beckmann 2004).

### 2.8. Target selection

fMRI analysis for each participant was completed before they arrived for their first TMS session. Two fMRI-based independent components, one that comprised the left FPN and one that comprised the posterior DMN, were visually identified from the output of ICA. Peak coordinates for the FPN and DMN were selected for each participant, targeting the left DLPFC and left angular gyrus, respectively. The average connectivity-based DLPFC MNI coordinate across subjects was X = −38, Y = 39, Z = 17. The average connectivity-based angular gyrus MNI coordinate across subjects was X = −44, Y = −58, Z = 32. Due to technical difficulties, the connectivity-based DLPFC session data for one participant and the angular gyrus excitation protocol session data for another participant were not saved, leaving 16 full datasets in those conditions.

For standardized target selection, peak voxels from a Neurosynth meta-analysis were used to locate the left DLPFC and left angular gyrus targets, based on the highest z-scores. MNI coordinates for Neurosynth-based DLPFC was X = −38, Y = 24, Z = 24. MNI coordinates for Neurosynth-based angular gyrus was X = −46, Y = −66, Z = 44. Although literature-driven coordinates were considered, the consensus on angular gyrus coordinates in TMS studies was limited, so we opted for the meta-analysis approach instead.

The average Euclidean distance between the DLPFC definitions was 16.55 mm across subjects with the individualized DLPFC targets more anterior on average to the Neurosynth based target definition (Fig. 1B). The average Euclidean distance between the angular gyrus definitions was 14.56 mm across subjects with the individual connectivity based angular gyrus targets being more anterior on average to the Neurosynth based target definition. The target for motor cortex stimulation was identified during identification of resting motor threshold at the beginning of each TMS session, following field-wide standards. Only one targeting method was used to stimulate the motor cortex.

### 2.9. TMS setup

TMS was delivered using a Magstim-200 stimulator connected to a co-planar figure-of-eight Magstim-P/N9925 induction coil with a 70-mm wing radius (The Magstim Company Ltd., Whitland, UK). MRI-guided neuronavigation was performed using the Brainsight Neuronavigation system to ensure precise cortical stimulation and to minimize variability in the stimulation location across sessions.

### 2.10. Resting motor threshold (RMT)

The location of motor cortex stimulation was determined first using iterative movement of the TMS coil and stimulation to locate the coordinates that stimulate the abductor pollicis brevis (APB) muscle representation in the left motor cortex. Once found, the resting motor threshold (RMT) at this site was identified using electromyography with a descending relative frequency approach to identify the threshold at which an MEP of at least 50 μV is achieved in at least 50% of 10 to 20 consecutive trials (Rossini et al., 1994, Rothwell et al., 1999).

### 2.11. TMS stimulation protocols

Motor cortex and each individual connectivity-defined target was stimulated using single-pulse and paired-pulse protocols. Neurosynth-defined targets were only stimulated using single-pulse protocol due to limitations on time and participant burden. The TMS coil was always held at an approximately 45 degrees angle relative to the midline. We used single-pulse and two paired-pulse protocols: short-interval intracortical inhibition (SICI) with a 3 ms interstimulus interval to probe inhibitory responses, and intracortical facilitation (ICF) with an 11 ms interval to assess excitatory processes. These intervals were selected based on prior work using similar timings in TMS-EEG (e.g., Lioumis et al., 2018) and are consistent with established ranges reported in the literature (Säisänen et al., 2011).

Stimulation intensity was set at 120% of the RMT for single-pulse TMS and at 80% (for the conditioning pulse) and 120% (for the test pulse) RMT for paired-pulse protocols (SICI and ICF). TMS was targeted for each region using MNI coordinates for each participant projected back into native space and then displayed on the participant's anatomical image during neuronavigation. Sixty pulses were applied per protocol at each target site, with interstimulus intervals jittered around 5 s. Inter-block intervals ranged between 2 and 5 min.

The order of stimulation sites and intensities remained the same for each participant across sessions but was pseudorandomized between participants (see Fig. 1C for an example sequence). This ensured that consecutive blocks were never over the same brain region, but any potential order effects remained constant within a participant.

Sham stimulation was introduced midway through the study and applied to a total of 11 participants. The primary rationale for including sham was to improve artifact removal during EEG preprocessing, particularly to aid in the identification of non-neural components during ICA decomposition. The sham protocol was implemented by tilting the TMS coil 90 degrees relative to the scalp such that the edge of the figure-of-eight coil touched the head while the coil center faced outward. In this configuration, the stimulator delivered pulses as in the real TMS conditions, but no effective magnetic field reached the cortex. This setup preserved the auditory and somatosensory sensations associated with TMS, without inducing cortical activation. This approach has been shown to aid in separating neural from non-neural components in preprocessing pipelines (Rogasch et al., 2014). The intensity of the sham blocks was 120% of the RMT.

### 2.12. TMS session procedures

During each session, participants were instructed to keep their eyes open and remain still throughout the recordings. For parietal cortex stimulations, participants rested their chin on a chin rest to maintain a stable head position throughout the procedure. Participants were instructed to keep their gaze steady but were allowed to move their eyes freely.

Neuronavigation ensured consistent coil positioning and orientation across both measurement sessions. The coil was manually held throughout the sessions and the distance error from the target per target region across subjects and sessions were as the following: motor cortex: 0.22 cm (SE = 0.02) DLPFC_RS: 0.23 cm (SE = 0.02); DLPFC_NS: 0.27 cm (SE = 0.03); AngularGyrus_RS: 0.29 cm (SE = 0.3); AngularGyrus_NS: 0.48 cm (SE = 0.17).

For motor cortex stimulation, the coil was positioned to elicit maximal motor-evoked potentials (MEPs) during the first session, and

this position was replicated in the second session. The twist error from the target angle per target region across subjects and sessions were as the following: motor cortex: 3.28° (SE = 1.07) DLPFC_RS: 0.10° (SE = 1.01); DLPFC_NS: 0.85° (SE = 0.90); AngularGyrus_RS: 2.06° (SE = 1.35); AngularGyrus_NS: 0.89° (SE = 1.38).

To reduce auditory contamination from the TMS click, we employed an individualized noise-masking procedure. During calibration, the coil was held approximately 10 cm above the vertex while participants listened to a scrambled version of the TMS click delivered through earphones. The volume of the noise was gradually increased until participants reported no longer perceiving the TMS click, within safe listening limits. Although this procedure does not eliminate bone conduction, it has been shown to significantly reduce auditory-evoked potentials and better isolate the cortical effects of TMS (Russo et al., 2022). We chose not to use a foam spacer or sponge between the coil and scalp, as it increases the distance to the cortex and consequently the required stimulation intensity, potentially affecting focality and participant comfort.

### 2.13. EEG recording

EEG responses to TMS were recorded using a 64-channel TMS-compatible EEG system (ActiChamp, Brain Products, GmbH, Germany) with passive electrodes designed to prevent overheating due to eddy currents induced by TMS. The EEG system was connected to a TMS-compatible amplifier with a sampling rate of 25 kHz, a bandwidth of 0.1–350 Hz, and a 16-bit AD conversion resolution. The EEG array was configured according to the international 10–20 system for optimal scalp coverage. EasyCap Abralyt HiCl High chloride abrasive electrolyte gel was used. Impedances were monitored after each session and the channels had impedances lower than 5 kΩ, ensuring good signal quality. The reference channel used during recording was Fz; the ground channel used during recording was FCz.

### 2.14. EEG data preprocessing

As part of the preprocessing workflow, the EEG data were segmented around each TMS pulse, with epochs spanning from −1.5 to 1.5 s relative to the test pulse in paired-pulse protocols. Baseline correction was applied differently for each protocol. For single-pulse protocols, baseline correction was performed using the interval from −500 to −5 ms before the pulse. For paired-pulse inhibition protocols, the baseline interval was adjusted to −500 to −8 ms before the test pulse, and for excitation protocols, it was adjusted to −500 to −16 ms before the test pulse. Condition-specific artifact removal was performed to address TMS-related noise. For single-pulse protocols, data from −2 to 5 ms were cut. For inhibition protocols, data from −5 to 5 ms before the test pulse were cut, and for excitation protocols, from −13 to 5 ms before the test pulse were cut. After this initial artifact removal, bad channels and trials were excluded to improve data quality. An average of 1.7 trials [0 11] ($SD$ = 3.90) and 0.77 channels [0 17] ($SD$ = 1.21) were rejected. The data were detrended and underwent baseline correction to remove any residual artifacts. Further processing included Independent Component Analysis (ICA). Data were reduced to 30 components to extract and remove eye blink, muscle, and line noise artifacts. For the second half of the sample, sham blocks were acquired per region and were concatenated to the end of real stimulation data during ICA separately for each stimulation site to help identify artifacts.

Although performing two rounds of ICA is a common practice in some preprocessing pipelines (e.g., TESA), we opted for a different approach based on the specific artifact profile of our data. In particular, we used a combination of the Source-estimate-utilizing noise-discarding algorithm ((SOUND, Mutanen et al., 2016) and Signal-space projection–source-informed reconstruction (SSP-SIR, Mutanen et al., 2016) methods to suppress large-amplitude, time-locked artifacts such as those arising from TMS-evoked muscle activity. This decision was motivated by the known limitations of ICA in handling time-locked signals, which violate the statistical independence assumption of ICA (Mutanen et al., 2024). SOUND–SSP–SIR has been shown to effectively suppress muscle and decay artifacts without compromising signal quality and has been used in recent studies for similar purposes (Bertazzoli et al., 2021). In our implementation, ICA was applied only once, primarily for the removal of ocular and residual non-neural artifacts. Given the risk of signal loss associated with multiple ICA passes, especially in the presence of strong muscle contamination, we considered this approach to be better suited for preserving cortical TMS-evoked activity in our dataset.

Hence, the SOUND algorithm was applied to suppress extracranial noise. The SSP-SIR method was used to reduce muscle artifacts induced by TMS. After artifact suppression, the missing time intervals were interpolated, and the data underwent bandpass filtering twice. Initially, to filter out frequencies outside the 1–100 Hz range and eliminate slow drifts. Subsequently, to remove line noise by applying a band-stop filter between 58 and 62 Hz.

### 2.15. TEP data analysis

To determine the time course of TMS-evoked potentials (TEPs) for each target region, we defined both large and small regions of interest (ROIs) based on sets of channels covering the DLPFC, motor cortex, and angular gyrus. Per each region, small and large ROI definitions were chosen (see Fig. 1D). Specific time windows (Fig. 1E) were chosen to optimize the capture of early neural responses in each target region, facilitating a comparison of TEP reliability across anatomically defined ROIs. Particularly, we extracted the maximum peak-to-peak amplitude within time windows defined based on previous literature (Gogulski et al 2024a, Gogulski et al 2024b) and adjusted according to the artifact profile of each stimulation site. Based on this prior research, we specifically focused on early local TMS-evoked potentials (EL-TEPs), as later components are more prone to artifacts.

For M1 stimulation, we used a time window of 10 to 40 ms, which captures early TEP components such as the N20 and N45. These components are reliably observed in M1 and are typically not obscured by TMS-related artifacts. For the DLPFC and parietal cortex, we used a later window of 20 to 60 ms. This shift was necessary to avoid contamination from early muscle artifacts and eye blinks, which are more prominent at frontal and parietal scalp sites following TMS (Rogasch et al., 2014; Biabani et al., 2019). These site-specific time windows enabled more accurate and reliable detection of early cortical responses across the different stimulation targets.

For each ROI, the peak-to-peak amplitude was calculated from the signal averaged across all channels within the ROI, rather than computing and averaging peak-to-peak values from individual channels. We computed the peak-to-peak amplitude by identifying the maximum and minimum values within the time window and calculating their difference. The resulting amplitude was then converted from linear microvolts (μV) to decibels (dB) using a logarithmic transformation, providing a consistent measure of TEP response strength across conditions.

This approach reduces the influence of channel-specific noise and provides a more stable estimate of the regional cortical response. Similar methods have been used in several previous TMS–EEG studies (Lioumis et al., 2009; Ilmoniemi and Kičić, 2010; Gordon et al., 2018; Rodionov et al., 2023; Gogulski et al., 2024). By averaging the signal prior to amplitude measurement, we aimed to improve the robustness and consistency of the extracted TEP features across participants and conditions.

To determine the test–retest reliability of TEPs at different time points, we used the Concordance Correlation Coefficient (CCC), a measure optimized for assessing test–retest reliability (Lawrence and Lin, 1989; Kerwin et al., 2018). The CCC compares the variance between subjects to the total variance to evaluate the agreement between two sets

of observations. In our analysis, we applied the CCC to quantify the reliability of TEPs across different stimulation conditions by comparing the magnitude of TEPs from one session to another session. Reliability was categorized as low (CCC $<$ 0.5), moderate (CCC between 0.5 and 0.7), or high (CCC $>$ 0.7). The CCC values were calculated for each target and time point, with mean values and 95% confidence intervals reported. To compare CCC values across conditions, we employed the percentile bootstrap method (Wilcox, 2009) to assess statistical differences in reliability (Gogulski et al., 2024a).

To complement the peak-to-peak amplitude analysis, we also computed the area under the curve (AUC) within the same time windows used for TEP quantification. CCCs calculated for the AUC values showed a similar pattern to the peak-to-peak results. These results further support the robustness of the regional differences observed in signal quality. Full CCC results are provided in the supplementary materials (Table S2, Figs. S2&3).

## 3. Results

In this study, we assessed the test–retest reliability of TEPs for functionally defined targets derived from the RMT procedure and fMRI. Specifically, we examined three left-lateralized brain regions—motor cortex (M1), dorsolateral prefrontal cortex (DLPFC), and angular gyrus—using three TMS protocols: single-pulse TMS, short-interval intracortical inhibition (SICI), and intracortical facilitation (ICF). For motor cortex, targets were defined using a standard RMT procedure. For DLPFC and angular gyrus, targets were defined using two methods: individual resting-state (RS) fMRI-based target localization and functional definition based on Neurosynth coordinates on normalized anatomical images. TEP reliability was assessed using the concordance correlation coefficient (CCC) for within-session and between-session reliability of the logarithmic peak-to-peak amplitude quantification within large ROIs, with bootstrapped confidence intervals (CIs) calculated for each CCC estimate (see Table S1 for smaller ROI definitions and linear values). See Figs. 1, 2, and 3 for the time course (Figs. 2 and 4) and scalp distribution (Fig. 3) of TEPs across all participants for each experimental condition.

### 3.1. Reliability across brain regions

TEP reliability varied across the three regions of interest (ROIs), with the highest CCC values observed in the motor cortex ($CCC_{mean}$ = 0.59, $CCC_{std}$ = 0.08) and lowest reliability scores for DLPFC ($CCC_{mean}$ = 0.40, $CCC_{std}$ = 0.15) and angular gyrus between them ($CCC_{mean}$ = 0.45, $CCC_{std}$ = 0.20). These results indicated that motor cortex stimulation overall produced the most consistent TEPs across regions (Fig. 5).

### 3.2. Reliability across target definitions

For DLPFC and angular gyrus, we compared reliability for targets

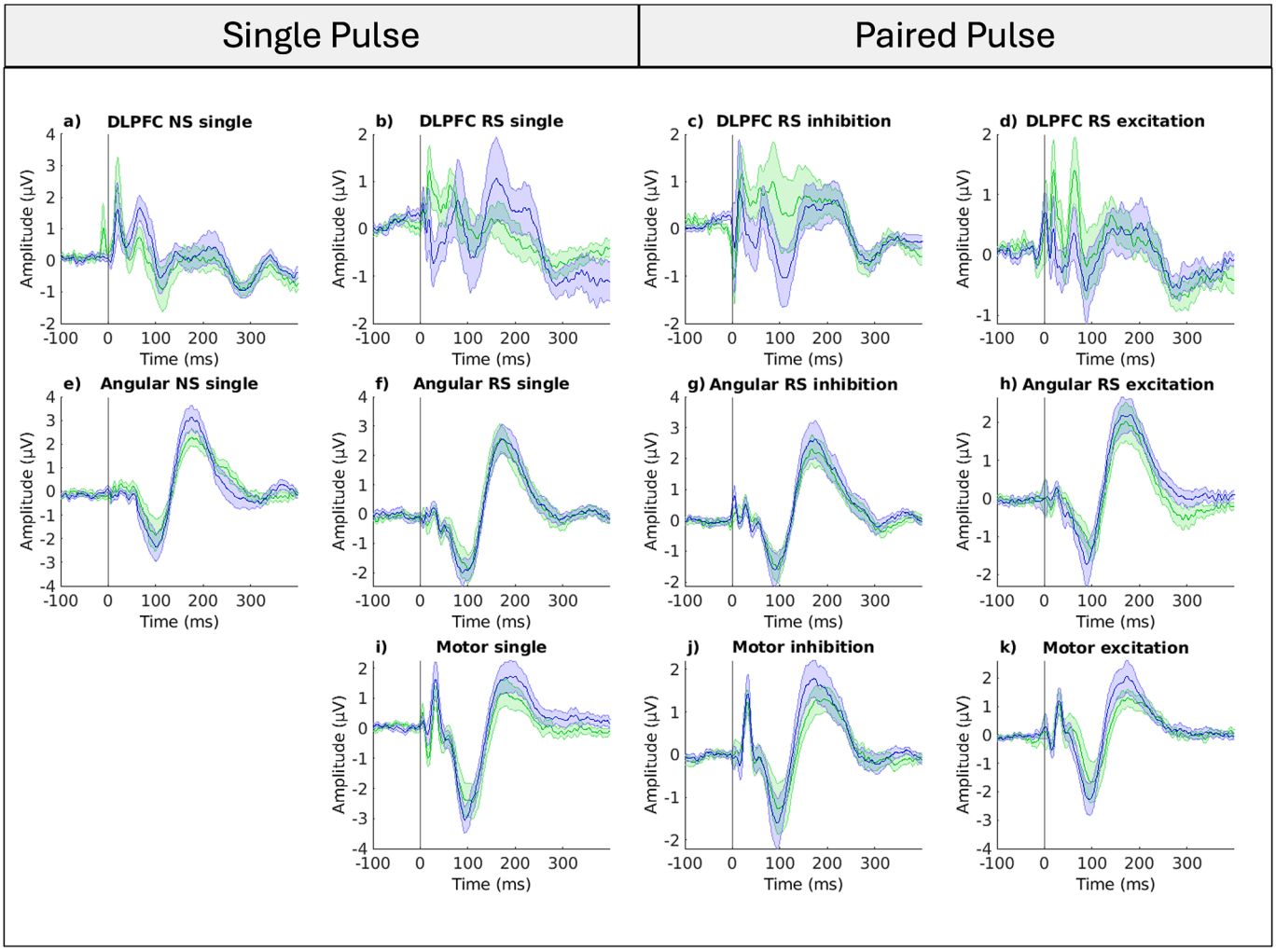


**Fig. 2.** Time course of TEPs across all participants for each experimental condition. Green lines stand for session 1 values; blue lines stand for session 2 values. Time is shown relative to the test pulse in excitation and inhibition conditions. RS: Resting State; NS: Neurosynth.

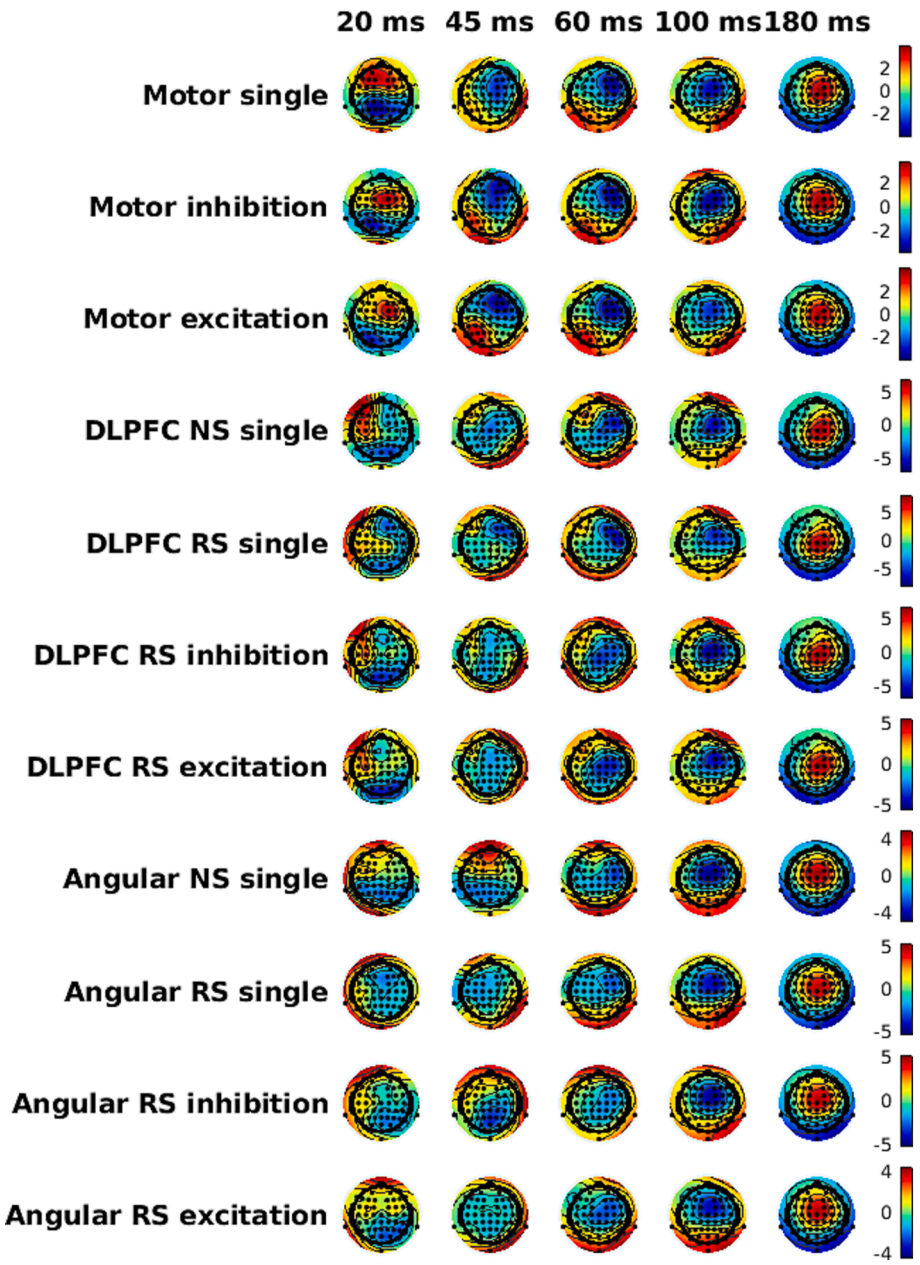


**Fig. 3.** Topographical maps across all participants and sessions for each experimental condition, averaged across sessions. Time is shown relative to the test pulse in excitation and inhibition conditions. RS: Resting State; NS: Neurosynth.

defined using RS and Neurosynth-derived functional overlays in the single pulse condition. Reliability for each experimental condition is presented in Table 1. Neurosynth-defined targets generally yielded higher CCC values in DLPFC with a mean CCC range of 0.57, CI [0.14 0.82], compared to RS derived targets, which showed a CCC range of 0.30, CI [−0.14 0.64] across sessions. However, the CCC difference between different DLPFC definitions was not significant, as revealed by bootstrap statistics ($CI_{difference}$ [−0.87 0.01], $P = 0.06$).

In angular gyrus, both target definitions showed moderate reliability with overlapping confidence intervals (Neurosynth-based: CCC = 0.30, CI [−0.19 0.67]; RS: CCC = 0.35, CI [−0.03 0.64]. The CCC difference between different angular gyrus definitions was not significant, as revealed by bootstrap statistics ($CI_{difference}$ [−0.55 0.70], $P = 0.83$).

### 3.3. Effect of TMS protocol on TEP reliability

There was no statistical difference between single-pulse and SICI ($CI_{difference}$ [−0.26 0.43], $P = 0.69$) or ICF ($CI_{difference}$ [−0.24 0.63], $P = 0.40$) conditions for M1. Similarly, there was no statistical difference between single-pulse and SICI ($CI_{difference}$ [−0.65 0.36], $P = 0.53$) or ICF ($CI_{difference}$ [−0.55 0.52], $P = 0.91$) conditions for DLPFC. There was also no statistical difference between single-pulse and SICI ($CI_{difference}$ [−0.52 0.43], $P = 0.93$) or ICF ($CI_{difference}$ [−0.86 0.04], $P = 0.08$) conditions for angular gyrus. These results indicate that all three TMS protocols have similar reliability across regions.

## 4. Discussion

The study primarily assessed the test–retest reliability of TEPs in the DLPFC and angular gyrus, with the motor cortex (M1) included as a standard benchmark for comparison. Three TMS protocols (single-pulse TMS, SICI, and ICF) and two target definition methods for DLPFC and angular gyrus (RS- and NS-based) were evaluated. Both the individual resting-state method and the Neurosynth method are based on

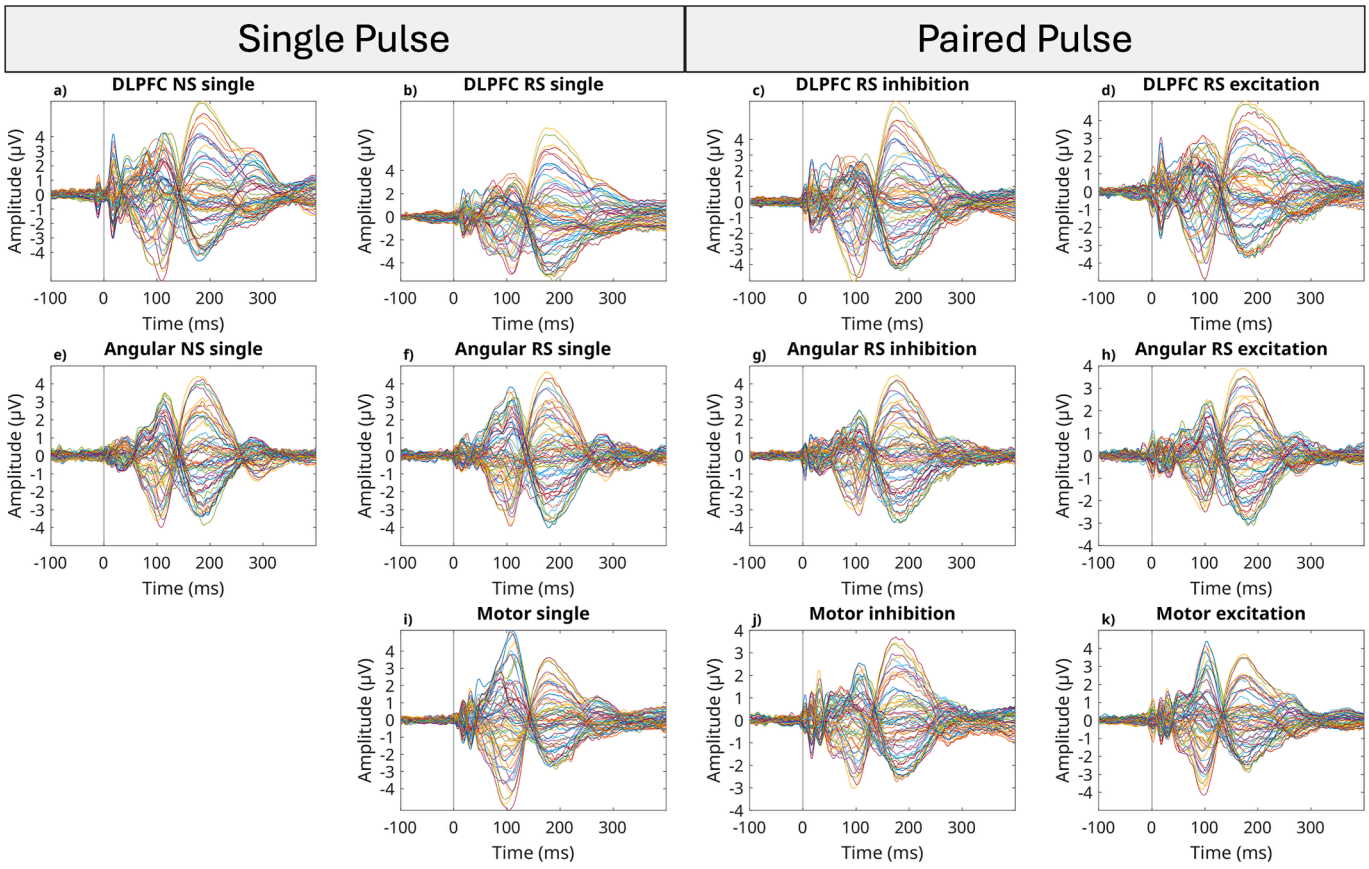


**Fig. 4.** Butterfly plots across all participants and sessions for each experimental condition averaged across sessions. Time is shown relative to the test pulse in excitation and inhibition conditions. RS: Resting State; NS: Neurosynth.

functional neuroimaging modalities. Results indicated that targeting DLPFC and angular gyrus using these methods did not yield TEPs as reliable as the standard RMT-based targeting method typically used for M1. While Neurosynth-derived targets demonstrated numerically higher CCC values for DLPFC compared to resting-state targets, this was not observed for the angular gyrus. Across all regions, no significant differences in reliability were found between the three TMS protocols. These findings suggest that individualized functional neuroimaging measures for targeting DLPFC and angular gyrus do not necessarily improve TEP reliability compared to the individualized RMT-based method.

Central targets, such as the motor cortex, are generally more reliable in TMS-EEG studies compared to targets like the DLPFC and angular gyrus, as the latter are more prone to muscle artifacts. Mutanen et al. (2013) demonstrated that early large biphasic deflections in TMS-evoked EEG signals are predominantly caused by cranial muscle activation rather than neural responses. Stimulation of areas overlying cranial muscles, such as the frontalis muscle for DLPFC and the temporalis muscle for angular gyrus, leads to pronounced artifacts, particularly in lateral EEG channels. These artifacts are sensitive to coil placement, orientation, and proximity to the muscles, making it challenging to isolate true neural responses. In contrast, central sites like the motor cortex are less affected by such confounds, providing cleaner EEG signals with higher reliability. Although strategies such as adjusting coil angles, reducing stimulation intensity, and employing offline artifact removal methods (e.g., independent component analysis or signal-space projection) can mitigate these artifact-derived issues, the inherent susceptibility of lateral targets to muscle-induced artifacts highlights the advantage of central targets for obtaining robust and artifact-free TEPs, and also the need of other strategies for the frontal and lateral targets.

Motor cortex also offers a clear functional readout in overt muscle movement, making it easier to find a precise location of stimulation in an individual. Such functional readouts are not readily available for cortical regions involved in complex cognition, such as DLPFC and angular gyrus. Thus, it may be that a more clear assessment of TEP reliability in these regions requires more careful identification of precise stimulation targets that will yield a clear TEP to begin with. The greater reliability of TEPs in the motor cortex compared to other regions may stem from the ability to optimize stimulation parameters in real time, and especially intensity and orientation, as assisted by real-time EMG readout. Similarly, real-time TEP software (Casarotto et al., 2022) provides immediate feedback on the quality of cortical responses by visualizing early EEG signals and detecting artifacts, enabling the adjustment of TMS parameters—such as site, orientation, and intensity—during and before data collection. Using this methodology in non-motor regions, such as the DLPFC and angular gyrus, may similarly enhance the reliability of TEPs by providing region-specific optimization (Parmigiani et al., 2025; Ukharova et al., JoVe, 2025; Lioumis et al., Frontiers, 2025). By leveraging real-time feedback, future studies could achieve individualized precision targeting for non-motor regions, reducing variability and increasing the reproducibility of TMS-EEG protocols across diverse cortical areas.

Our findings align with and expand upon the observations reported by Gogulski et al. (2024a) regarding the influence of target selection within the DLPFC on TEP reliability. In our study, we found that the connectivity-based DLPFC target, which was more anterior compared to the Neurosynth-based target, exhibited numerically smaller TEP amplitudes and lower test–retest reliability. This pattern is consistent with Gogulski et al (2024a) observation that more anterior DLPFC targets often produce smaller amplitude EL-TEPs and, in some cases, lower reliability. While smaller amplitudes may reflect reduced neural engagement or increased susceptibility to artifacts at anterior sites, the

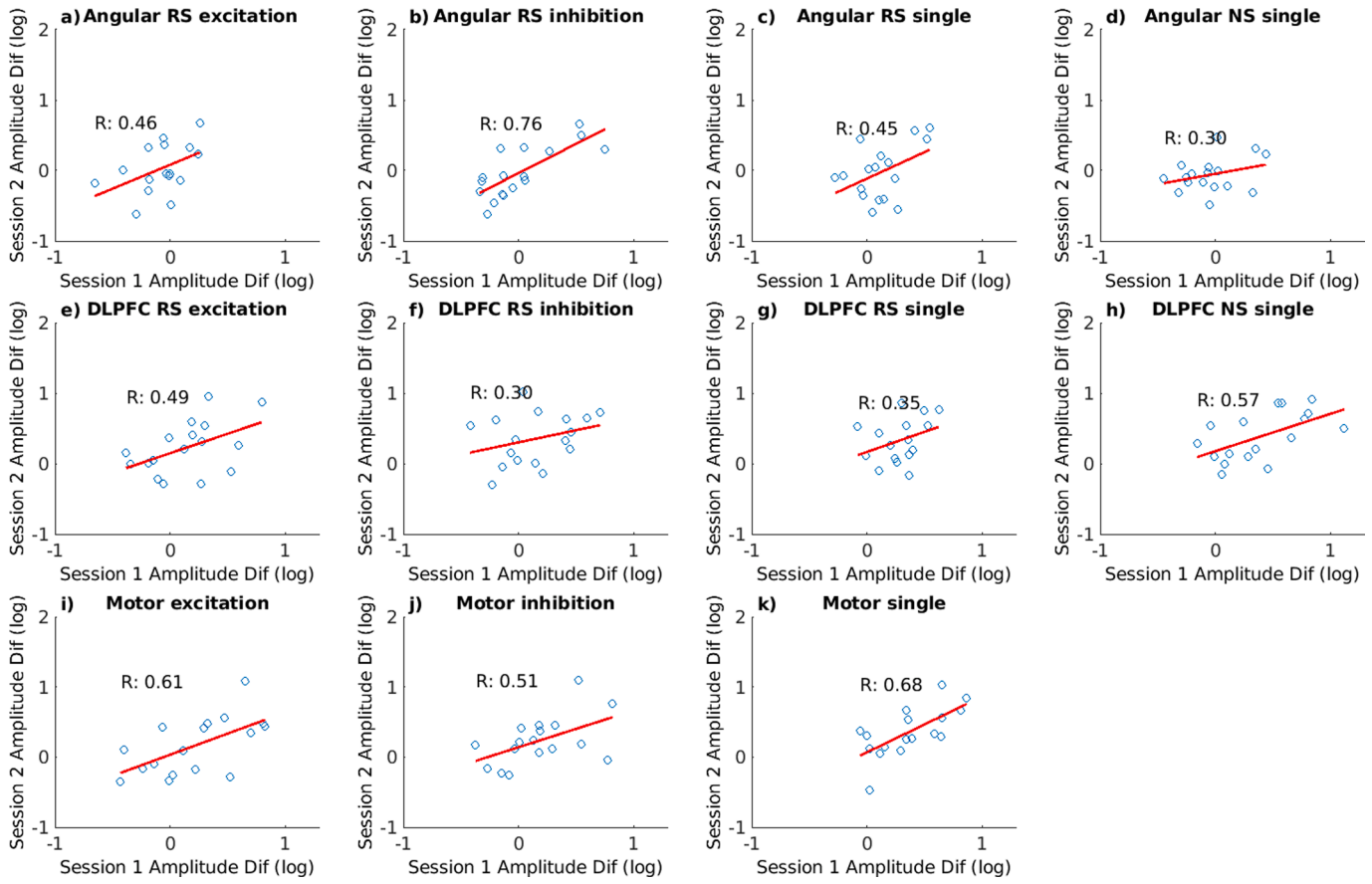


**Fig. 5.** Scatter plot of log-transformed amplitude differences, calculated by taking the difference between maximum and minimum peak-to-peak amplitudes within a time window, between sessions across experimental conditions. R values stand for Pearson product moment correlation coefficients. RS: Resting State; NS: Neurosynth.

**Table 1**
Reliability of TEPs between session 1 and session 2, across experimental condition. CCC: concordance correlation coefficient; CI: 95% confidence interval; Mean Amp: mean amplitude of the signal within selected time windows; RS: Resting State; NS: Neurosynth.

| | CCC | low CI | high CI | Mean Amp |
|---|---|---|---|---|
| Angular RS excitation | 0.40 | −0.03 | 0.71 | −0.03 |
| Angular RS inhibition | 0.75 | 0.44 | 0.90 | −0.01 |
| Angular RS single | 0.35 | −0.03 | 0.64 | 0.05 |
| Angular NS single | 0.30 | −0.19 | 0.67 | −0.05 |
| DLPFC RS excitation | 0.47 | 0.02 | 0.76 | 0.18 |
| DLPFC RS inhibition | 0.25 | −0.17 | 0.59 | 0.25 |
| DLPFC RS single | 0.30 | −0.14 | 0.64 | 0.31 |
| DLPFC NS single | 0.57 | 0.14 | 0.82 | 0.39 |
| Motor excitation | 0.60 | 0.19 | 0.83 | 0.19 |
| Motor inhibition | 0.51 | 0.06 | 0.78 | 0.21 |
| Motor single | 0.67 | 0.31 | 0.86 | 0.36 |

relationship between amplitude and reliability is not straightforward. Our results suggest that functionally guided targeting, such as connectivity-based approaches, may require careful validation to optimize both amplitude magnitude and reliability, particularly when stimulating anterior DLPFC regions.

Our findings also align with Kerwin et al. (2018) in demonstrating the influence of trial number, target location, and temporal interval on TMS-EEG reliability. In our study, we used 60 trials per condition and observed a CCC of 0.57 for DLPFC targets, which is lower than the substantial concordance (>0.8) reported by Kerwin et al. for peaks such as N100 and P200. Kerwin et al. noted that while even 20 trials may suffice for high concordance in short-interval test–retest designs (within the same session), greater trial numbers are required for longer temporal intervals, such as separate-day comparisons. Our study employed a one-week interval between sessions which, alongside the relatively low trial number, may have contributed to the reduced reliability, particularly for early components such as the N20 and N45 and for non-central targets like the DLPFC and angular gyrus, consistent with Lioumis et al., 2009. Moreover, consistent with their findings, we observed that target location plays a critical role, with the motor cortex exhibiting the highest reliability, comparable to the high concordance Kerwin et al. (2018) reported for central regions. This highlights the impact of both experimental parameters and regional variability on TEP reliability, suggesting that increasing trial numbers and optimizing stimulation targets could improve reliability in future studies.

Stimulation intensity may also play a critical role in minimizing artifacts and optimizing TEP reliability. In our study, we employed a standardized approach, using predetermined percentages of RMT such as 120% and 80% RMT for our protocols, which aligns with common clinical practices. However, Mutanen et al. (2013) highlight that such intensities, while effective for clinical applications, may not be optimal for TEP studies. They demonstrated that reducing stimulation intensity from 100% to 60–80% of the motor threshold led to an 80–90% reduction in muscle artifacts, which are a major source of noise in TEP recordings.

Finally, preprocessing of the EEG data may have contributed to signal quality. EEG data were preprocessed manually using a stepwise approach tailored to the specific characteristics of each dataset. While automated preprocessing pipelines can enhance reproducibility, they may apply fixed thresholds that are not optimal for datasets with high variability or complex artifact profiles. In our case, manual

preprocessing allowed us to make informed decisions regarding trial and channel rejection criteria based on overall signal quality and the number of usable trials per participant. This approach also facilitated close inspection of the data, which we consider essential for distinguishing genuine cortical responses from artifacts.

We tested several automated pipelines, including ARTIST and TESA, but found that they removed nearly all TMS-evoked signal in our data. This is likely because our stimulation targets were defined based on individual fMRI activation and not optimized for minimizing EEG artifacts. As a result, strong muscle activity near the stimulation site led these automated pipelines to over-clean the data, removing signal components of interest. By using manual preprocessing, we were able to retain meaningful neural signals while suppressing non-neural artifacts through careful inspection and targeted cleaning.

Our findings highlight the distinction between target engagement in fMRI-guided TMS studies and the reliability challenges inherent in TMS-EEG studies. While fMRI-based approaches prioritize functional connectivity to maximize engagement of specific brain networks, such as the DLPFC-subgenual cingulate connection in depression treatment, TMS-EEG studies must contend with confounds like TMS-induced muscle artifacts, which often obscure the true neural signal (Casarotto et al., 2022; Lioumis and Rosanova, 2022). Consequently, TMS-EEG research should focus on identifying stimulation sites that yield the highest signal-to-noise ratio (SNR; Tervo et al., 2022) rather than strictly aligning with fMRI-defined connectivity targets. This difference underscores that the optimal target for fMRI-based studies may not correspond to the most reliable TEP signal in TMS-EEG studies.

Lioumis and Rosanova (2022) propose a potential solution to reconcile these approaches by integrating navigated TMS with tractography and other neuroimaging techniques and high-density EEG, which has been demonstrated recently in DLPFC (Ukharova et al., JoVe, 2025) and in the SMA complex (Lioumis et al., Frontiers, 2025). This method could simultaneously map the structural, functional, and connectional profiles of a target area, optimizing both target engagement and TEP reliability, by potentially ensuring stimulating the desired cytoarchitectonics. Such an approach addresses the limitations of relying solely on connectivity-based targets, as it ensures that the anatomical and functional signatures of a stimulation site are jointly considered. By combining TMS-fMRI's ability to engage functional networks with TMS-EEG's focus on signal reliability, future studies can better align the objectives of target engagement and artifact-free neurophysiological measurements. This integrative framework represents a promising avenue for advancing the utility of TMS-EEG-based biomarkers while maintaining the precision of individualized targeting.

## Availability of data and materials

Data is available to share upon request.

## Declaration of competing interest

The authors declare the following financial interests/personal relationships which may be considered as potential competing interests: FSB has received research funding from the Wana Brand Foundation, is a scientific advisor for WavePaths, Ltd, has received compensation as a consultant for Gilgamesh Pharmaceuticals, Inc, and has received compensation as a consultant for and holds stock in MindState Design Labs, LLC. CS has received a gift from the Sidar Sahin Foundation. IG has received consulting fees from Nexstim Plc unrelated to this work. JG has received a lecture fee from Orion Pharma Oyj unrelated to this work. PL is a consultant to Nexstim Plc for TMS–EEG applications and speech cortical mapping.

## Acknowledgements

This work was supported by the Johns Hopkins Center for Psychedelic and Consciousness Research, which was funded by a generous gift from the Steven and Alexandra Cohen Foundation as well as Tim Ferriss, Matt Mullenweg, Blake Mycoskie, and Craig Nerenberg. We thank Christopher Cline for providing scripts for data visualization. We also thank Daniel Galvez Cabrera and Sean Garcy for their assistance with data collection.

### *Funding*

This work was supported by the Johns Hopkins Center for Psychedelic and Consciousness Research, which was funded by a generous gift from the Steven and Alexandra Cohen Foundation as well as Tim Ferriss, Matt Mullenweg, Blake Mycoskie, and Craig Nerenberg. IG has received funding from the Swedish Cultural Foundation and from the Finnish Cultural Foundation and by the Research Council Finland (357660). JG was supported by a personal grant from Emil Aaltonen Foundation, Finnish Medical Foundation, Sigrid Jusélius Foundation, and Instrumentarium Science Foundation and by the Research Council Finland (357660). PL was supported by Wellcome Leap as part of the Multi-Channel Psych Program and has also received funding from the European Research Council (ERC) under the European Union's Horizon 2020 Research Innovation Programme (grant agreement No 81037)

### *Code availability*

The authors will upload all relevant analysis code on a public repository.

### *Authors' contributions*

CS and FB conceptualized the work. FB provided the funding for the study. CS collected and analyzed the data. DJ, EW, and GL preprocessed the EEG data. JG, IG and PL provided support for data analysis and interpretation of data. All authors wrote, revised, and approved of the final manuscript.

### *Consent to participate*

All human subjects provided informed consent to participate in this study.

### *Consent for publication*

All human subjects provided informed consent to publish this research.

## Appendix A. Supplementary data

Supplementary material includes tables reporting concordance correlation coefficients (CCCs) across all stimulation conditions (excitation, inhibition, single-pulse), target sites (angular gyrus, DLPFC, motor cortex), and small and large ROI definitions. Supplementary data to this article can be found online at https://doi.org/10.1016/j.clinph.2026.2112327.

## References

Avants, B.B., Epstein, C.L., Grossman, M., Gee, J.C., 2008. Symmetric diffeomorphic image registration with cross-correlation: evaluating automated labeling of elderly and neurodegenerative brain. Med. Image Anal. 12 (1), 26–41.

Balderston, N.L., Beer, J.C., Seok, D., Makhoul, W., Deng, Z.D., Girelli, T., Sheline, Y.I., 2022. Proof of concept study to develop a novel connectivity-based electric-field modelling approach for individualized targeting of transcranial magnetic stimulation treatment. Neuropsychopharmacology 47 (2), 588–598.

Beam, W., Borckardt, J.J., Reeves, S.T., George, M.S., 2009. An efficient and accurate new method for locating the F3 position for prefrontal TMS applications. Brain Stimul. 2 (1), 50–54.

Beckmann, C. F. (2004, April). Probabilistic ICA for fMRI. In 2004 2nd IEEE International Symposium on Biomedical Imaging: Nano to Macro (IEEE Cat No. 04EX821) (pp. 1490-1493). IEEE.
Bertazzoli, G., Esposito, R., Mutanen, T.P., Ferrari, C., Ilmoniemi, R.J., Miniussi, C., Bortoletto, M., 2021. The impact of artifact removal approaches on TMS–EEG signal. Neuroimage 239, 118272.
Beynel, L., Gura, H., Rezaee, Z., Ekpo, E.C., Deng, Z.D., Joseph, J.O., Lisanby, S.H., 2024. Lessons learned from an fMRI-guided rTMS study on performance in a numerical Stroop task. PLoS One 19 (5), e0302660.
Biabani, M., Fornito, A., Mutanen, T., Morrow, J., Rogasch, N., 2019. Sensory contamination in TMS-EEG recordings: can we isolate TMS-evoked neural activity? Brain Stimul. 12 (2), 473.
Bodart, O., Gosseries, O., Wannez, S., Thibaut, A., Annen, J., Boly, M., Laureys, S., 2017. Measures of metabolism and complexity in the brain of patients with disorders of consciousness. NeuroImage: Clinical 14, 354–362.
Boroojerdi, B., Foltys, H., Krings, T., Spetzger, U., Thron, A., Töpper, R., 1999. Localization of the motor hand area using transcranial magnetic stimulation and functional magnetic resonance imaging. Clin. Neurophysiol. 110 (4), 699–704.
Buckner, R.L., Andrews-Hanna, J.R., Schacter, D.L., 2008. The brain's default network: anatomy, function, and relevance to disease. Ann. N. Y. Acad. Sci. 1124 (1), 1–38.
Canali, P., 2014. A role for TMS/EEG in neuropsychiatric disorders. Neurol. Psychiatry Brain Res. 20 (2), 37–40.
Canali, P., Casarotto, S., Rosanova, M., Sferrazza-Papa, G., Casali, A.G., Gosseries, O., Benedetti, F., 2017. Abnormal brain oscillations persist after recovery from bipolar depression. Eur. Psychiatry 41 (1), 10–15.
Canali, P., Sarasso, S., Rosanova, M., Casarotto, S., Sferrazza-Papa, G., Gosseries, O., Benedetti, F., 2015. Shared reduction of oscillatory natural frequencies in bipolar disorder, major depressive disorder and schizophrenia. J. Affect. Disord. 184, 111–115.
Casali, A.G., Gosseries, O., Rosanova, M., Boly, M., Sarasso, S., Casali, K.R., Massimini, M., 2013. A theoretically based index of consciousness independent of sensory processing and behavior. Sci. Transl. Med. 5 (198), 198ra105-198ra105.
Casarotto, S., Canali, P., Rosanova, M., Pigorini, A., Fecchio, M., Mariotti, M., Massimini, M., 2013. Assessing the effects of electroconvulsive therapy on cortical excitability by means of transcranial magnetic stimulation and electroencephalography. Brain Topogr. 26, 326–337.
Casarotto, S., Comanducci, A., Sarasso, S., Fecchio, M., Rosanova, M., Massimini, M., 2017. The potential of nTMS/EEG: measuring consciousness. Navigated Transcranial Magnetic Stimulation in Neurosurgery 257–265.
Casarotto, S., Fecchio, M., Rosanova, M., Varone, G., D'Ambrosio, S., Sarasso, S., Massimini, M., 2022. The rt-TEP tool: real-time visualization of TMS-Evoked Potentials to maximize cortical activation and minimize artifacts. J. Neurosci. Methods 370, 109486.
Casarotto, S., Romero Lauro, L.J., Bellina, V., Casali, A.G., Rosanova, M., Pigorini, A., Massimini, M., 2010. EEG responses to TMS are sensitive to changes in the perturbation parameters and repeatable over time. PLoS One 5 (4), e10281.
Cash, R.F., Cocchi, L., Lv, J., Wu, Y., Fitzgerald, P.B., Zalesky, A., 2021. Personalized connectivity-guided DLPFC-TMS for depression: advancing computational feasibility, precision and reproducibility. Hum. Brain Mapp. 42 (13), 4155–4172.
Cieslik, E.C., Seidler, I., Laird, A.R., Fox, P.T., Eickhoff, S.B., 2016. Different involvement of subregions within dorsal premotor and medial frontal cortex for pro-and antisaccades. Neurosci. Biobehav. Rev. 68, 256–269.
Cieslik, E.C., Zilles, K., Caspers, S., Roski, C., Kellermann, T.S., Jakobs, O., Eickhoff, S.B., 2013. Is there "one" DLPFC in cognitive action control? Evidence for heterogeneity from co-activation-based parcellation. Cereb. Cortex 23 (11), 2677–2689.
Conde, V., Tomasevic, L., Akopian, I., Stanek, K., Saturnino, G.B., Thielscher, A., Siebner, H.R., 2019. The non-transcranial TMS-evoked potential is an inherent source of ambiguity in TMS-EEG studies. Neuroimage 185, 300–312.
Dale, A., Fischl, B., Sereno, M.I., 1999. Cortical surface-based analysis: I. Segmentation and surface reconstruction. Neuroimage 9 (2), 179–194. https://doi.org/10.1006/nimg.1998.0395.
Daskalakis, Z.J., Farzan, F., Barr, M.S., Maller, J.J., Chen, R., Fitzgerald, P.B., 2008. Long-interval cortical inhibition from the dorsolateral prefrontal cortex: a TMS–EEG study. Neuropsychopharmacology 33 (12), 2860–2869.
Dengler, J., Deck, B.L., Stoll, H., Fernandez-Nunez, G., Kelkar, A.S., Rich, R.R., Medaglia, J.D., 2024. Enhancing cognitive control with transcranial magnetic stimulation in subject-specific frontoparietal networks. Cortex 172, 141–158.
Desrochers, T.M., Chatham, C.H., Badre, D., 2015. The necessity of rostrolateral prefrontal cortex for higher-level sequential behavior. Neuron 87 (6), 1357–1368.
Esteban, O., Markiewicz, C.J., Blair, R.W., Moodie, C.A., Isik, A.I., Erramuzpe, A., Kent, J. D., Goncalves, M., DuPre, E., Snyder, M., Oya, H., Ghosh, S.S., Wright, J., Durnez, J., Poldrack, R.A., Gorgolewski, K.J., 2018. fMRIPrep: a robust preprocessing pipeline for functional MRI. Nat Meth. https://doi.org/10.1038/s41592-018-0235-4.
Farzan, F., Barr, M.S., Wong, W., Chen, R., Fitzgerald, P.B., Daskalakis, Z.J., 2009. Suppression of γ-oscillations in the dorsolateral prefrontal cortex following long interval cortical inhibition: a TMS–EEG study. Neuropsychopharmacology 34 (6), 1543–1551.
Ferrarelli, F., Phillips, M.L., 2021. Examining and modulating neural circuits in psychiatric disorders with transcranial magnetic stimulation and electroencephalography: present practices and future developments. Am. J. Psychiatry 178 (5), 400–413.
Fitzgerald, P.B., Maller, J.J., Hoy, K., Farzan, F., Daskalakis, Z.J., 2009. GABA and cortical inhibition in motor and non-motor regions using combined TMS–EEG: a time analysis. Clin. Neurophysiol. 120 (9), 1706–1710.
Fox, M.D., Buckner, R.L., White, M.P., Greicius, M.D., Pascual-Leone, A., 2012. Efficacy of transcranial magnetic stimulation targets for depression is related to intrinsic functional connectivity with the subgenual cingulate. Biol. Psychiatry 72 (7), 595–603.
Gogulski, J., Cline, C.C., Ross, J.M., Parmigiani, S., Keller, C.J., 2024a. Reliability of the TMS-evoked potential in dorsolateral prefrontal cortex. Cereb. Cortex 34 (4), bhae130.
Gogulski, J., Cline, C.C., Ross, J.M., Truong, J., Sarkar, M., Parmigiani, S., Keller, C.J., 2024b. Mapping cortical excitability in the human dorsolateral prefrontal cortex. Clin. Neurophysiol.: Off. J. Int. Federat. Clin. Neurophysiol. 164, 138–148. https://doi.org/10.1016/j.clinph.2024.05.008.
Gorgolewski, K., Burns, C.D., Madison, C., Clark, D., Halchenko, Y.O., Waskom, M.L., Ghosh, S.S., 2011 Aug 22. Nipype: a flexible, lightweight and extensible neuroimaging data processing framework in python. Front. Neuroinf. 5 (August), 13. https://doi.org/10.3389/fninf.2011.00013.
Gorgolewski KJ, Esteban O, Ellis DG, Notter MP, Ziegler E, Johnson H, Hamalainen C, Yvernault B, Burns C, Manhães-Savio A, Jarecka D, Markiewicz CJ, Salo T, Clark D, Waskom M, Wong J, Modat M, Dewey BE, Clark MG, Dayan M, Loney F, Madison C, Gramfort A, Keshavan A, Berleant S, Pinsard B, Goncalves M, Clark D, Cipollini B, Varoquaux G, Wassermann D, Rokem A, Halchenko YO, Forbes J, Moloney B, Malone IB, Hanke M, Mordom D, Buchanan C, Pauli WM, Huntenburg JM, Horea C, Schwartz Y, Tungaraza R, Iqbal S, Kleesiek J, Sikka S, Frohlich C, Kent J, Perez-Guevara M, Watanabe A, Welch D, Cumba C, Ginsburg D, Eshaghi A, Kastman E, Bougacha S, Blair R, Acland B, Gillman A, Schaefer A, Nichols BN, Giavasis S, Erickson D, Correa C, Ghayoor A, Küttner R, Haselgrove C, Zhou D, Craddock RC, Haehn D, Lampe L, Millman J, Lai J, Renfro M, Liu S, Stadler J, Glatard T, Kahn AE, Kong X-Z, Triplett W, Park A, McDermottroe C, Hallquist M, Poldrack R, Perkins LN, Noel M, Gerhard S, Salvatore J, Mertz F, Broderick W, Inati S, Hinds O, Brett M, Durnez J, Tambini A, Rothmei S, Andberg SK, Cooper G, Marina A, Mattfeld A, Urchs S, Sharp P, Matsubara K, Geisler D, Cheung B, Floren A, Nickson T, Pannetier N, Weinstein A, Dubois M, Arias J, Tarbert C, Schlamp K, Jordan K, Liem F, Saase V, Harms R, Khanuja R, Podranski K, Flandin G, Papadopoulos Orfanos D, Schwabacher I, McNamee D, Falkiewicz M, Pellman J, Linkersdörfer J, Varada J, Pérez-García F, Davison A, Shachnev D, Ghosh S. Nipype: a flexible, lightweight and extensible neuroimaging data processing framework in Python. 2017. doi:10.5281/zenodo.581704.
Greve, D.N., Fischl, B., 2009 Oct. Accurate and robust brain image alignment using boundary-based registration. Neuroimage 48 (1), 63–72. https://doi.org/10.1016/j.neuroimage.2009.06.060.
Gordon, P.C., Zrenner, C., Desideri, D., Belardinelli, P., Zrenner, B., Brunoni, A.R., Ziemann, U., 2018. Modulation of cortical responses by transcranial direct current stimulation of dorsolateral prefrontal cortex: a resting-state EEG and TMS-EEG study. Brain Stimul. 11 (5), 1024–1032.
Hallett, M., 2000. Transcranial magnetic stimulation and the human brain. Nature 406 (6792), 147–150.
Harquel, S., Bacle, T., Beynel, L., Marendaz, C., Chauvin, A., David, O., 2016. Mapping dynamical properties of cortical microcircuits using robotized TMS and EEG: Towards functional cytoarchitectonics. Neuroimage 135, 115–124.
Hawco, C., Voineskos, A.N., Steeves, J.K., Dickie, E.W., Viviano, J.D., Downar, J., Daskalakis, Z.J., 2018. Spread of activity following TMS is related to intrinsic resting connectivity to the salience network: a concurrent TMS-fMRI study. Cortex 108, 160–172.
Herbsman, T., Avery, D., Ramsey, D., Holtzheimer, P., Wadjik, C., Hardaway, F., Nahas, Z., 2009. More lateral and anterior prefrontal coil location is associated with better repetitive transcranial magnetic stimulation antidepressant response. Biol. Psychiatry 66 (5), 509–515.
Hernandez-Pavon, J.C., Veniero, D., Bergmann, T.O., Belardinelli, P., Bortoletto, M., Casarotto, S., Ilmoniemi, R.J., 2023. TMS combined with EEG: Recommendations and open issues for data collection and analysis. Brain Stimul. 16 (2), 567–593.
Herwig, U., Satrapi, P., Schönfeldt-Lecuona, C., 2003. Using the international 10-20 EEG system for positioning of transcranial magnetic stimulation. Brain Topogr. 16, 95–99.
Horvath, J. C., Mathews, J., Demitrack, M. A., & Pascual-Leone, A. (2010). The NeuroStar TMS device: conducting the FDA approved protocol for treatment of depression. Journal of visualized experiments: JoVE, (45).
Hoshi, E., 2006. Functional specialization within the dorsolateral prefrontal cortex: a review of anatomical and physiological studies of non-human primates. Neurosci. Res. 54 (2), 73–84.
Hui, J., Zomorrodi, R., Lioumis, P., Salavati, B., Rajji, T.K., Chen, R., Daskalakis, Z.J., 2020. Pharmacological mechanisms of interhemispheric signal propagation: a TMS-EEG study. Neuropsychopharmacology 45 (6), 932–939.
Hyvarinen, A., 1999. Fast and robust fixed-point algorithms for independent component analysis. IEEE Trans. Neural Netw. 10 (3), 626–634.
Ilmoniemi, R.J., Kičić, D., 2010. Methodology for combined TMS and EEG. Brain Topogr. 22 (4), 233–248.
Ilmoniemi, R.J., Virtanen, J., Ruohonen, J., Karhu, J., Aronen, H.J., Näätänen, R., Katila, T., 1997. Neuronal responses to magnetic stimulation reveal cortical reactivity and connectivity. Neuroreport 8 (16), 3537–3540.
Jenkinson, M., Bannister, P., Brady, M., Smith, S., 2002 Oct. Improved optimization for the robust and accurate linear registration and motion correction of brain images. Neuroimage 17 (2), 825–841. https://doi.org/10.1006/nimg.2002.1132.
Kerwin, L.J., Keller, C.J., Wu, W., Narayan, M., Etkin, A., 2018. Test-retest reliability of transcranial magnetic stimulation EEG evoked potentials. Brain Stimul. 11 (3), 536–544.
Klein, A., Ghosh, S.S., Bao, F.S., Giard, J., Häme, Y., Stavsky, E., et al., 2017. Mindboggling morphometry of human brains. PLoS Comput. Biol. 13 (2), e1005350. https://doi.org/10.1371/journal.pcbi.1005350.

Komssi, S., Aronen, H.J., Huttunen, J., Kesäniemi, M., Soinne, L., Nikouline, V.V., Ilmoniemi, R.J., 2002. Ipsi-and contralateral EEG reactions to transcranial magnetic stimulation. Clin. Neurophysiol. 113 (2), 175–184.
Krings, T., Buchbinder, B.R., Butler, W.E., Chiappa, K.H., Jiang, H.J., Rosen, B.R., Cosgrove, G.R., 1997. Stereotactic transcranial magnetic stimulation: correlation with direct electrical cortical stimulation. Neurosurgery 41 (6), 1319–1326.
Lawrence, I., Lin, K., 1989. A concordance correlation coefficient to evaluate reproducibility. Biometrics 255–268.
Lioumis, P., Roine, T., Granö, I., Aydogan, D.B., Ukharova, E., Souza, V.H., Kičić, D., Ilmoniemi, R.J., Makris, N., 2025. Optimization of TMS target engagement: current state and future perspectives. Front. Neurosci. 19, 1517228. https://doi.org/10.3389/fnins.2025.1517228.
Lioumis, P., Rosanova, M., 2022. The role of neuronavigation in TMS–EEG studies: current applications and future perspectives. J. Neurosci. Methods 380, 109677.
Lioumis, P., Kičić, D., Savolainen, P., Mäkelä, J.P., Kähkönen, S., 2009. Reproducibility of TMS—Evoked EEG responses. Hum. Brain Mapp. 30 (4), 1387–1396.
Lioumis, P., Zomorrodi, R., Hadas, I., Daskalakis, Z.J., Blumberger, D.M., 2018. Combined transcranial magnetic stimulation and electroencephalography of the dorsolateral prefrontal cortex. J. Visual. Exp.: JoVE 138, 57983.
Mäki, H., Ilmoniemi, R.J., 2011. Projecting out muscle artifacts from TMS-evoked EEG. Neuroimage 54 (4), 2706–2710.
Mutanen, T.P., Kukkonen, M., Nieminen, J.O., Stenroos, M., Sarvas, J., Ilmoniemi, R.J., 2016. Recovering TMS-evoked EEG responses masked by muscle artifacts. Neuroimage 139, 157–166.
Mutanen, T., Mäki, H., Ilmoniemi, R.J., 2013. The effect of stimulus parameters on TMS–EEG muscle artifacts. Brain Stimul. 6 (3), 371–376.
Mutanen, T.P., Ilmoniemi, I., Atti, I., Metsomaa, J., Ilmoniemi, R.J., 2024. A simulation study: comparing independent component analysis and signal-space projection–source-informed reconstruction for rejecting muscle artifacts evoked by transcranial magnetic stimulation. Front. Hum. Neurosci. 18, 1324958.
Nee, D.E., D'Esposito, M., 2017. Causal evidence for lateral prefrontal cortex dynamics supporting cognitive control. Elife 6, e28040.
Noda, Y., Zomorrodi, R., Cash, R.F., Barr, M.S., Farzan, F., Rajji, T.K., Blumberger, D.M., 2017. Characterization of the influence of age on GABAA and glutamatergic mediated functions in the dorsolateral prefrontal cortex using paired-pulse TMS-EEG. Aging (Albany NY) 9 (2), 556.
Nord, C.L., 2021. Predicting response to brain stimulation in depression: a roadmap for biomarker discovery. Curr. Behav. Neurosci. Rep. 8, 11–19.
Oathes, D.J., Balderston, N.L., Kording, K.P., DeLuisi, J.A., Perez, G.M., Medaglia, J.D., Linn, K.A., 2021a. Combining transcranial magnetic stimulation with functional magnetic resonance imaging for probing and modulating neural circuits relevant to affective disorders. Wiley Interdiscip. Rev. Cogn. Sci. 12 (4), e1553.
Oathes, D.J., Zimmerman, J.P., Duprat, R., Japp, S.S., Scully, M., Rosenberg, B.M., Linn, K.A., 2021b. Resting fMRI-guided TMS results in subcortical and brain network modulation indexed by interleaved TMS/fMRI. Exp. Brain Res. 239, 1165–1178.
Oliver, L.D., Hawco, C., Viviano, J.D., Voineskos, A.N., 2022. From the group to the individual in schizophrenia spectrum disorders: biomarkers of social cognitive impairments and therapeutic translation. Biol. Psychiatry 91 (8), 699–708.
Parmigiani, S., Cline, C.C., Sarkar, M., Forman, L., Truong, J., Ross, J.M., Keller, C.J., 2025. Real-time optimization to enhance noninvasive cortical excitability assessment in the human dorsolateral prefrontal cortex. Clin. Neurophysiol.
Pascual-Leone, A., Walsh, V., Rothwell, J., 2000. Transcranial magnetic stimulation in cognitive neuroscience–virtual lesion, chronometry, and functional connectivity. Curr. Opin. Neurobiol. 10 (2), 232–237.
Paus, T., Jech, R., Thompson, C.J., Comeau, R., Peters, T., Evans, A.C., 1997. Transcranial magnetic stimulation during positron emission tomography: a new method for studying connectivity of the human cerebral cortex. J. Neurosci. 17 (9), 3178–3184.
Pellicciari, M.C., Veniero, D., Miniussi, C., 2017. Characterizing the cortical oscillatory response to TMS pulse. Front. Cell. Neurosci. 11, 38.
Radhu, N., Blumberger, D. M., & Daskalakis, Z. J. (2016). Cortical Inhibition and excitation in neuropsychiatric disorders using transcranial magnetic stimulation. Transcranial Direct Current Stimulation in Neuropsychiatric Disorders: Clinical Principles and Management, 85-102.
Radhu, N., Dominguez, L.G., Greenwood, T.A., Farzan, F., Semeralul, M.O., Richter, M. A., Daskalakis, Z.J., 2017. Investigating cortical inhibition in first-degree relatives and probands in schizophrenia. Sci. Rep. 7 (1), 43629.
Rodionov, A., Ozdemir, R.A., Benwell, C.S., Fried, P.J., Boucher, P., Momi, D., Shafi, M. M., 2023. Reliability of resting-state EEG modulation by continuous and intermittent theta burst stimulation of the primary motor cortex: a sham-controlled study. Sci. Rep. 13 (1), 18898.
Rogasch, N.C., Thomson, R.H., Farzan, F., Fitzgibbon, B.M., Bailey, N.W., Hernandez-Pavon, J.C., Fitzgerald, P.B., 2014. Removing artefacts from TMS-EEG recordings using independent component analysis: importance for assessing prefrontal and motor cortex network properties. Neuroimage 101, 425–439.
Rogasch, N.C., Daskalakis, Z.J., Fitzgerald, P.B., 2015. Cortical inhibition of distinct mechanisms in the dorsolateral prefrontal cortex is related to working memory performance: a TMS–EEG study. Cortex 64, 68–77.
Rossini, P.M., Barker, A.T., Berardelli, A., Caramia, M.D., Caruso, G., Cracco, R.Q., Tomberg, C., 1994. Non-invasive electrical and magnetic stimulation of the brain, spinal cord and roots: basic principles and procedures for routine clinical application. Report of an IFCN committee. Electroencephalogr. Clin. Neurophysiol. 91 (2), 79–92.
Rothwell, J.C., Hallett, M., Berardelli, A., Eisen, A., Rossini, P., Paulus, W., 1999. Magnetic stimulation: motor evoked potentials. the international federation of clinical neurophysiology. Electroencephalogr. Clin. Neurophysiol. Suppl. 52, 97–103.
Rusjan, P. M., Barr, M. S., Farzan, F., Arenovich, T., Maller, J. J., Fitzgerald, P. B., & Daskalakis, Z. J. (2010). Optimal transcranial magnetic stimulation coil placement for targeting the dorsolateral prefrontal cortex using novel magnetic resonance image-guided neuronavigation (Vol. 31, No. 11, pp. 1643-1652). Hoboken: Wiley Subscription Services, Inc., A Wiley Company.
Russo, S., Sarasso, S., Puglisi, G.E., Dal Palù, D., Pigorini, A., Casarotto, S., Fecchio, M., 2022. TAAC-TMS adaptable auditory control: a universal tool to mask TMS clicks. J. Neurosci. Methods 370, 109491.
Sack, A.T., Kadosh, R.C., Schuhmann, T., Moerel, M., Walsh, V., Goebel, R., 2009. Optimizing functional accuracy of TMS in cognitive studies: a comparison of methods. J. Cogn. Neurosci. 21 (2), 207–221.
Sack, A.T., Kohler, A., Linden, D.E., Goebel, R., Muckli, L., 2006. The temporal characteristics of motion processing in hMT/V5+: combining fMRI and neuronavigated TMS. Neuroimage 29 (4), 1326–1335.
Säisänen, L., Julkunen, P., Niskanen, E., Hukkanen, T., Mervaala, E., Karhu, J., Könönen, M., 2011. Short-and intermediate-interval cortical inhibition and facilitation assessed by navigated transcranial magnetic stimulation. J. Neurosci. Methods 195 (2), 241–248.
Shafi, M.M., Whitfield-Gabrieli, S., Chu, C.J., Pascual-Leone, A., Chang, B.S., 2016. A Multimodal imaging-and stimulation-based method of evaluating connectivity-related brain excitability in patients with epilepsy. J. Visual. Exp.: JoVE 117, 53727.
Sparing, R., Buelte, D., Meister, I.G., Paus, T., Fink, G.R., 2008. Transcranial magnetic stimulation and the challenge of coil placement: a comparison of conventional and stereotaxic neuronavigational strategies. Hum. Brain Mapp. 29, 82–96.
Steinmetz, H., Seitz, R.J., 1991. Functional anatomy of language processing: neuroimaging and the problem of individual variability. Neuropsychologia 29 (12), 1149–1161.
Sun, Y., Farzan, F., Mulsant, B.H., Rajji, T.K., Fitzgerald, P.B., Barr, M.S., Daskalakis, Z.J., 2016. Indicators for remission of suicidal ideation following magnetic seizure therapy in patients with treatment-resistant depression. JAMA Psychiat. 73 (4), 337–345.
Tervo, A.E., Nieminen, J.O., Lioumis, P., Metsomaa, J., Souza, V.H., Sinisalo, H., Ilmoniemi, R.J., 2022. Closed-loop optimization of transcranial magnetic stimulation with electroencephalography feedback. Brain Stimul. 15 (2), 523–531.
Tremblay, S., Rogasch, N.C., Premoli, I., Blumberger, D.M., Casarotto, S., Chen, R., Daskalakis, Z.J., 2019. Clinical utility and prospective of TMS–EEG. Clin. Neurophysiol. 130 (5), 802–844.
Tustison, N.J., Avants, B.B., Cook, P.A., Zheng, Y., Egan, A., Yushkevich, P.A., Gee, J.C., 2010. N4ITK: improved N3 bias correction. IEEE Trans. Med. Imaging 29 (6), 1310–1320.
Ukharova, E., Sathyan, S., Granö, I., O'Meeghan, I., Ahola, O., Kainulainen, N., Laurinoja, J., Partanen, P., Aydogan, D.B., Ilmoniemi, R.J., Roine, T., Lioumis, P., 2025. Neuroimaging-Guided TMS-EEG for Real-Time Cortical Network Mapping. J. Visual. Exp.: JoVE 220. https://doi.org/10.3791/67339.
Valentin, A., Arunachalam, R., Mesquita-Rodrigues, A., Garcia Seoane, J.J., Richardson, M.P., Mills, K.R., Alarcon, G., 2008. Late EEG responses triggered by transcranial magnetic stimulation (TMS) in the evaluation of focal epilepsy. Epilepsia 49 (3), 470–480.
Veniero, D., Bortoletto, M., Miniussi, C., 2009. TMS-EEG co-registration: on TMS-induced artifact. Clin. Neurophysiol. 120 (7), 1392–1399.
Weigand, A., Horn, A., Caballero, R., Cooke, D., Stern, A.P., Taylor, S.F., Fox, M.D., 2018. Prospective validation that subgenual connectivity predicts antidepressant efficacy of transcranial magnetic stimulation sites. Biol. Psychiatry 84 (1), 28–37.
Wilcox, R.R., 2009. Robust ANCOVA using a smoother with bootstrap bagging. Br. J. Math. Stat. Psychol. 62 (2), 427–437.
Wilson, S.A., Thickbroom, G.W., Mastaglia, F.L., 1993. Transcranial magnetic stimulation mapping of the motor cortex in normal subjects: the representation of two intrinsic hand muscles. J. Neurol. Sci. 118 (2), 134–144.
Yeo, B.T., Krienen, F.M., Sepulcre, J., Sabuncu, M.R., Lashkari, D., Hollinshead, M., Buckner, R.L., 2011. The organization of the human cerebral cortex estimated by intrinsic functional connectivity. J. Neurophysiol.